A Multi-objective Co-Design Optimization Framework for Grid-Connected Hybrid Battery Energy Storage Systems: Optimal Sizing and Selection of Technology

Mahamudul Hasan, Boris Berseneff, Tim Meulenbroeks, Igor Cantero, Sajib Chakraborti, Thomas Geury, Omar Hegazy

energies

MDPI

Article

A Multi-Objective Co-Design Optimization Framework for Grid-Connected Hybrid Battery Energy Storage Systems: Optimal Sizing and Selection of Technology

Md. Mahamudul Hasan [1,2,*], Boris Berseneff [3], Tim Meulenbroeks [4], Igor Cantero [5], Sajib Chakraborty [1,2], Thomas Geury [1,2] and Omar Hegazy [1,2]

[1] MOBI-EPOWERS Research Group, ETEC Department, Vrije Universiteit Brussel, Pleinlaan 2, 1050 Brussels, Belgium; sajib.chakraborty@vub.be (S.C.); thomas.geury@vub.be (T.G.); omar.hegazy@vub.be (O.H.)
[2] Flanders Make, Gaston Geenslaan 8, 3001 Heverlee, Belgium
[3] Cea-Liten, Universités Grenoble Alpes, 38000 Grenoble, France; boris.berseneff@cea.fr
[4] Department of Powertrains, TNO, 5700 AT Helmond, The Netherlands; tim.meulenbroeks@tno.nl
[5] Cegasa Energia S.L.U., 01015 Vitoria, Spain; icantero@cegasa.com
* Correspondence: md.mahamudul.hasan@vub.be

Abstract: This paper develops a multi-objective co-design optimization framework for the optimal sizing and selection of battery and power electronics in hybrid battery energy storage systems (HBESSs) connected to the grid. The co-design optimization approach is crucial for such a complex system with coupled subcomponents. To this end, a nondominated sorting genetic algorithm (NSGA-II) is used for optimal sizing and selection of technologies in the design of the HBESS, considering design parameters such as cost, efficiency, and lifetime. The interoperable framework is applied considering three first-life battery cells and one second-life battery cell for forming two independent battery packs as a hybrid battery unit and considers two power conversion architectures for interfacing the hybrid battery unit to the grid with different power stages and levels of modularity. Finally, the globally best HBESS system obtained as the output of the framework is made up of LTO first-life and LFP second-life cells and enables a total cost of ownership (TCO) reduction of 29.6% compared to the baseline.

Keywords: BESS; optimal sizing; co-design optimization; hybrid battery energy storage system; Li-ion battery; HBESS; LiB grid storage system

Citation: Hasan, M.M.; Berseneff, B.; Meulenbroeks, T.; Cantero, I.; Chakraborty, S.; Geury, T.; Hegazy, O. A Multi-Objective Co-Design Optimization Framework for Grid-Connected Hybrid Battery Energy Storage Systems: Optimal Sizing and Selection of Technology. *Energies* **2022**, *15*, 5355. https://doi.org/10.3390/en15155355

Academic Editor: Chunhua Liu

Received: 27 June 2022
Accepted: 21 July 2022
Published: 24 July 2022

1. Introduction

The European Green Deal is expected to have zero net emission of greenhouse gases by 2050, when economic growth will be decoupled from resource use. Besides, the grid-related global storage systems deployment was about 10 GWh in 2019 and is projected to increase 15 times to almost 160 GWh with the deployment of 31.2 GWh in the EU and 34.3 GWh in the USA by 2030 [1]. A study in [2] also indicates that 150 to 900 million electric vehicles are expected to be on the market in 2040 and that stationary storage may reach up to 1300 GWh at that time. These projections point toward the potentially significant market growth of Li-ion batteries and a view of action against climate change by decarbonizing. However, the cost reduction of a lithium-ion battery (LIB) pack is slower in the stationary storage sector than in electric vehicles. In 2017, the benchmark costs of Li-ion stationary storage systems were approximately 500 EUR/kWh for energy-designed systems, 800 EUR/kWh for power-designed systems, and 750 EUR/kWh for residential batteries [2]. By 2040, stationary storage system costs are anticipated to range from 165–240 EUR/kWh for the energy-focused grid-connected system, while power-focused and residential systems are expected to cost 280–410 EUR/kWh and 250–365 EUR/kWh, respectively [2,3].

It is also found that for a battery-based system with more than 90% efficiency and a lifetime of thousands of cycles, the system cost is expected to be below 150 EUR/kWh (for a 100 kW reference system) in 2030 [4].

The different types of battery energy storage system (BESS) technologies and their suitability to grid-relieving applications have been presented in several research works with respect to efficiency, power, energy density, response time, cost, and other performance indicators [5–7]. Despite recent price reductions in Li-ion cells, the battery is one of the primary cost drivers of BESSs [6].

The standard stationary energy storage systems that use a single type of battery pack technology are able to supply services to the grid; however, a trade-off must often be made between power and energy performances [8]. It is found that most types of BESS and power electronics (PE) interfaces either have significant energy or power needs [9–12]; sizing one type of battery pack to multiple use cases is challenging. For example, by connecting additional cells in series/parallel, a single battery pack technology can provide the power and energy demands. However, the cells cannot be connected arbitrarily because of the voltage and current limits imposed by the PE interfaces. These current and voltage constraints increase complexity in design and contribute to oversizing the battery pack, resulting in either a higher power-to-energy ratio or a higher energy-to-power ratio. It should be noted that in most commercial battery systems, a greater energy-to-power battery pack is preferred since more energy in the battery pack increases longevity while reducing the strain on the cells. However, because of oversizing, this method is not cost-effective.

In contrast to this single-pack approach, a hybrid battery unit uses at least two different types of cells, which enhances the sizing and design possibilities. For example, combining a high-energy (HE) pack and a high-power (HP) pack enables to cover more applications for an interoperable service portfolio. Such a strategy increases the flexibility in sizing and thus the possibility of the economy of scales, which may help reduce the TCO.

There are different types of LIB technologies on the market, including the increasingly large number of second-life modules coming from the electric vehicle (EV) sector [13]. The LIB cells are mainly identified by name as lithium cobalt oxide (LCO), lithium manganese oxide (LMO), lithium iron phosphate (LFP), lithium nickel cobalt aluminum oxide (NCA), lithium nickel manganese cobalt oxide (NMC), and lithium titanate oxide (LTO). They have distinct cell voltage, energy density, cycle life, and cost because of their internal structure and composition [14]. Four types of lithium-ion cells are considered in this paper to cope with the high power and high energy demand in grid services.

The design optimization of BESSs is usually carried out regarding sizing, grid integration, technical performance, and economic perspective. In ref. [15], a single type of battery energy storage system was created from sodium sulfur (NaS), lead acid (LA), and vanadium redox (VR) and its related power converters to maximize profit for an EV park owner, using linear programming to identify the ideal storage size. The objective function includes cycle life and cost. In ref. [16], authors optimized and evaluated the BESS size for wind and solar energy fluctuations using genetic algorithm (GA). Optimizing the BESS installation capacity helps reduce power outage costs, fuel costs, and committed power plant costs. According to ref. [17], BESSs have issues with investment costs and operating lifetimes; therefore, adequate BESS sizing is crucial for microgrid design and administration. This article proposed a problem structure and solution approach for calculating the optimal size of BESSs in a microgrid using the binary particle swarm optimization (BPSO) combined with a quadratic programming algorithm for two objectives—investment cost and operating cost. Furthermore, to solve other multi-objective problems, such as minimization of annual net profits, energy consumptive rate, annual energy exchanged with the grid, and battery degradation, the NSGA-II algorithm has been utilized in [18,19]. To deal with BESS sizing, other optimization algorithms such as ant colony, particle swarm, and simulated annealing have been reviewed for multi-objective problems with different constraints based on different applications [20]. Among the other used algorithms, the

NSGA-II and its derivative algorithms are found to be the popular ones in multi-objective optimization problem solving [21].

However, a multi-objective genetic algorithm (MOGA) can be used for nonlinear, non-convex, discrete, continuous, mixed-integer, and multiple objective optimization problems [20,22]. For certain rule-based energy management methods, previous research optimized HBESS size. However, many studies [23,24] have focused on developing control strategies for the BESS sizing to achieve certain economic objectives, such as maximizing profit and minimizing power loss or battery degradation. In contrast, a system-level optimization technique is realized through the design of integrated subcomponents of HBESS and advanced control strategies, as it is necessary to know not only the revenue to maximize but also the upfront cost of investments, taking into account potential replacements over the system time horizon. In terms of assessment, the total ownership cost model has been used in [25,26] for BESS.

At the time of writing, to the authors' best knowledge, a generalized co-design optimization framework (COF) for a lithium-ion HBESS design in a grid application has not been developed yet. In this work, each battery pack is sized from cell to pack level along with the sizing of the power converter system (PCS) for interfacing the battery system to the grid. In this paper, the sizing of the battery pack is referred to as cell configuration of series-parallel to the battery pack rating in power and energy. The sizing of PCS is referred to the required rating and value for different PCS topologies.

The main contribution of this work is three-fold: (a) first, instead of a single type of battery pack technology, two distinct battery packs have been sized with the optimal combination of series-parallel cells out of four lithium-ion battery technologies for the HBESS design; (b) second, a novel and interoperable multi-objective optimization methodology with a co-design approach is developed for the optimal design, selection, and sizing of the HBESS subcomponents (battery and PCS) with respect to system-level techno-economic performance (i.e., cost, roundtrip efficiency, and lifetime); and (c) third, two different PCS architectures with modularity have been incorporated to interface the battery to the grid instead of a single PCS architecture.

This paper is organized as follows. The methodology for sizing and designing an optimal HBESS applicable for COF is introduced in Section 2. The detailed modeling required for the coupled HBESS simulation in the COF is described in Section 3. Besides, the processes for implementing the optimization routine of multi-objective COF are discussed in Section 4 to find the optimal storage system sizing and selection; a real-field grid service (i.e., UK grid service) power profile for enhanced frequency support is used in the framework to find the optimal sizing and selection of technology for HBESS from the selected four types of cells and two distinct PCSs. The optimization results and global best selection are presented in Section 5. Finally, the conclusions are outlined in Section 6.

2. System Description

This section presents the system considered for the framework shown in Figure 1. A synergic design goal with nominal power of 100 kW and nominal capacity of 100 kWh HBESS with two different PCS topologies (defined in an optimization routine, Section 4) is set in the COF to define its variables presented in Table 1. The COF is applied to the DC side of the system for an optimal hybridization of cell technologies for two independent battery packs, namely battery pack-1 and battery pack-2, and to the PE interface with two distinct architectures, PCS-1 and PCS-2.

The first architecture (PCS-1) is comprised of a DC/DC stage and a DC/AC stage as a single module to connect the grid with different battery modules for bidirectional charging and discharging functionalities, as highlighted in Figure 1. A modular PCS has been considered in the COF to find the optimal number of modules to be used for the HBESS.

In the second PCS architecture (PCS-2), the modular DC/DC stage is connected with the modular DC/AC stage through a single DC-link capacitor, as highlighted in Figure 1, which also enables bidirectional power flow between the hybrid BESS and the grid.

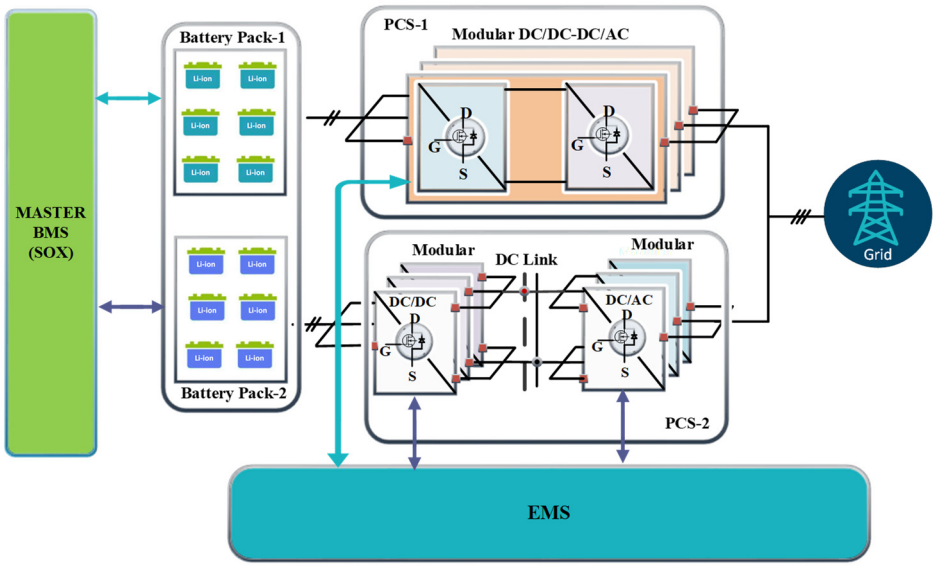

Figure 1. Principle schematic of the considered HBESS.

Table 1. Notations used to define the size of HBESS.

Notations	Descriptions
$N_s \times N_p$	Number of cells in series and parallel for each battery pack configuration
V_{Nom}	Nominal voltage for each battery pack
E_{bp}	Battery pack energy
P_m^{pe1}	Power rating of PCS-1 module
N_m^{pe1}	Number of PCS-1 module
$P_{mAC/DC}^{pe2}$	Power rating of PCS-2 AC/DC module
$P_{mDC/DC}^{pe1}$	Power rating of PCS-2 DC/DC module
V_{dclink}^{pe1}	DC-link voltage for PCS-2 module
$N_{mAC/DC}^{pe1}$	Number of PCS-2 AC/DC modules
$N_{mDC/DC}^{pe1}$	Number of PCS-2 DC/DC modules

The optimal voltage rating of the DC-link capacitor and the number of modules of the DC/DC and DC/AC stages for PCS-2 will be the outcome of the COF for the designed system. The details of the PCS architecture specification and constraints defined for HBESS are presented in Section 4.

The battery pack is sized by optimizing the number of cells in series and parallel. In the battery storage unit, two independent battery packs are sized where one acts as a high-power pack and the other one acts as a high-energy pack, considering different cell technologies. To this extent, this paper will propose an optimized battery storage unit based on the combination of battery pack-1 (high-energy) and battery pack-2 (high-power) to obtain the optimum level of power and energy of the battery for the considered mission power profile.

The design simulation framework, the COF, is prepared with a MATLAB/Simulink® environment and incorporates design optimization-oriented battery models and PCS models coupled with an operational control plant, namely an energy management system (EMS) for optimal sizing and selection.

2.1. Connection Topology (TO) of the HBESS

The specific connection configuration of the BESS affects the system performances, such as efficiency and reliability [27]. Considering both conceivable PCS architectures and their characteristics, four different connection topologies have been incorporated into the COF for individual selection or all at once while sizing the HBESS. The configurations are mentioned as follows in the remainder of the paper:

- TO-1: Both battery packs are connected to the grid using PCS-1, as shown in Figure 2.
- TO-2: Both battery packs are connected to the grid using PCS-2, as shown in Figure 3.
- TO-3: Battery pack-1 is connected to the grid using PCS-2, while battery pack-2 is connected using PCS-1, as shown in Figure 4.
- TO-4: Battery pack-1 is connected to the grid using PCS-1, while battery pack-2 is connected using PCS-2, as shown in Figure 5.

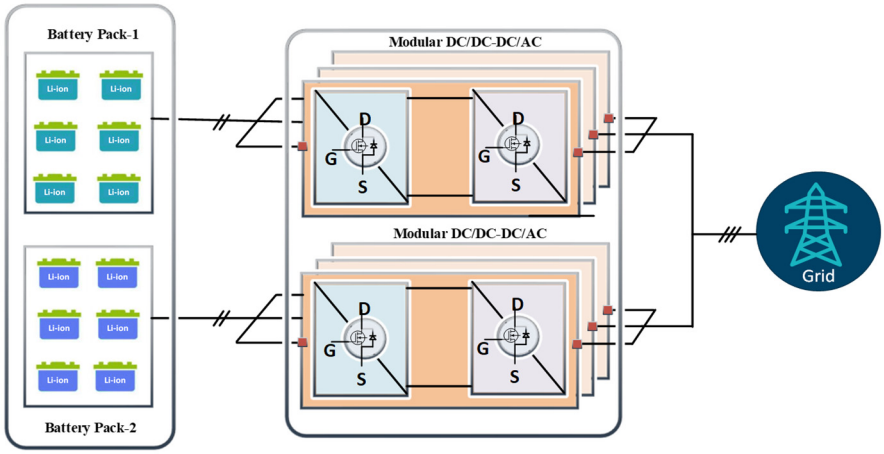

Figure 2. PE configuration 1: only PCS-1 is used.

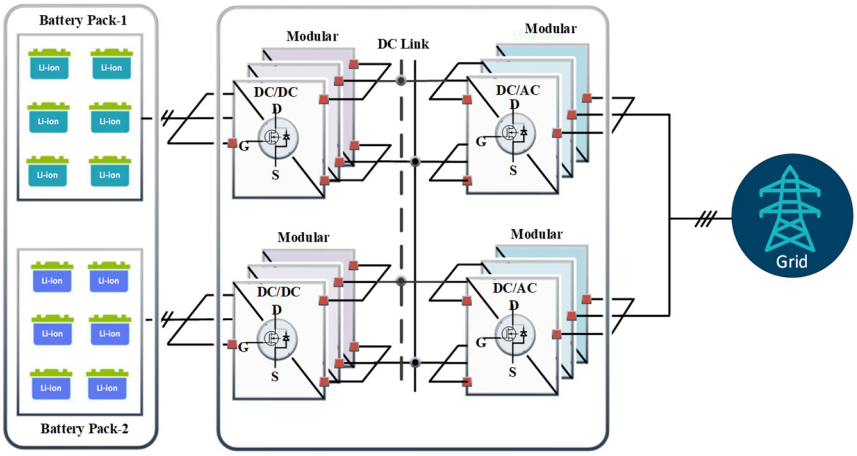

Figure 3. PE configuration 2: only PCS-2 is used.

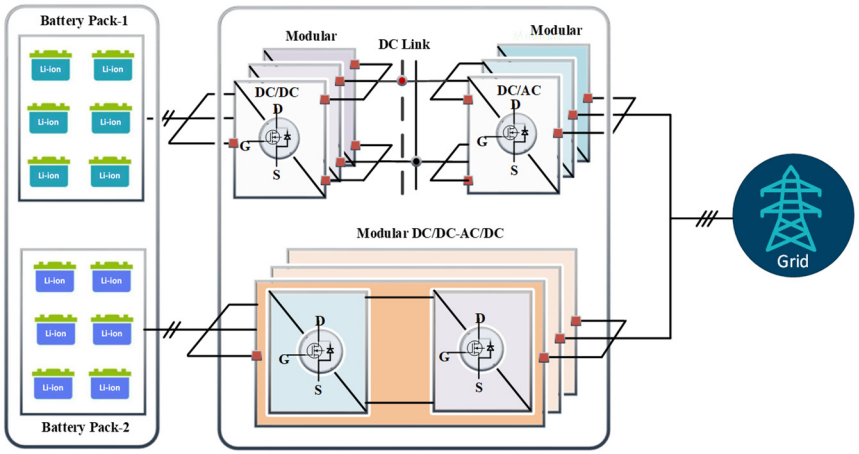

Figure 4. PE configuration 3: PCS-2 for battery pack-1 and PCS-1 for battery pack-2.

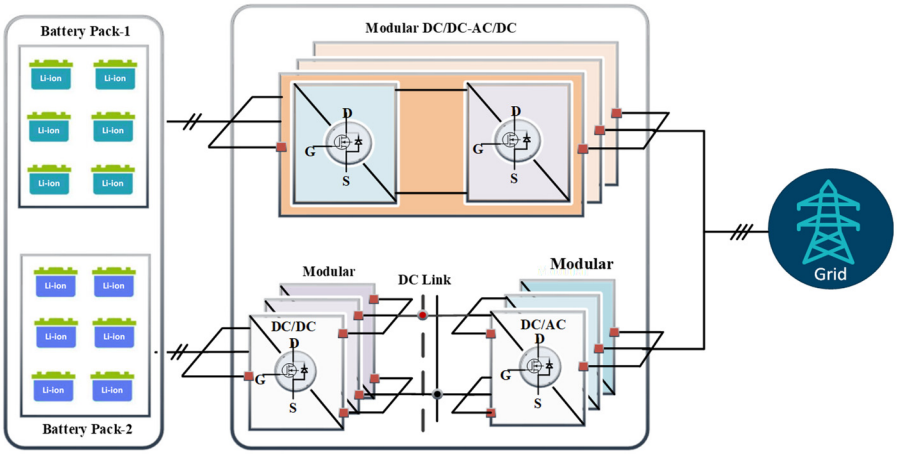

Figure 5. PE configuration 4: PCS-1 for battery pack-1 and PCS-2 for battery pack-2.

2.2. Real-Field Grid Load Profile for Case Study

The HBESS is subjected to multiple service scenarios. The framework considers a real-field grid-related service power profile [28]. The power profile dynamics from the UK grid services in enhanced frequency support have been considered in the COF. The power-to-frequency characteristic enables the conversion of recorded frequency variations to the required output/input power on a second-by-second basis, as shown in Figure 6.

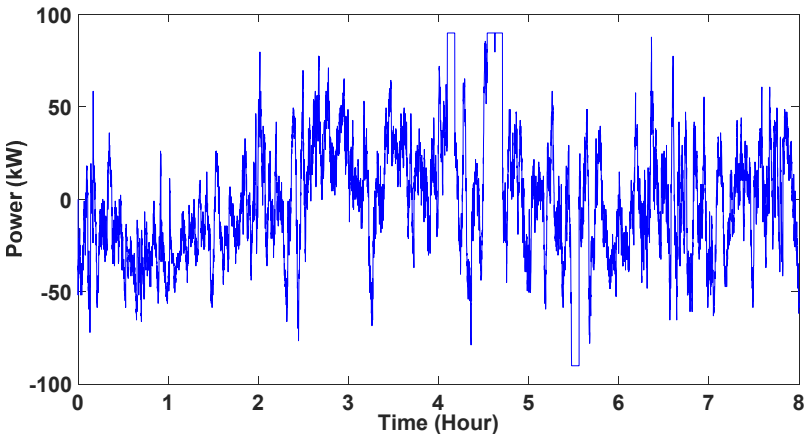

Figure 6. Eight-hour UK grid service profile to be used in the COF.

3. Modeling for COF

This section describes the simulation models of the batteries and PE interfaces incorporated in the COF for the optimal design and sizing of the HBESS.

3.1. Battery Model

The COF uses battery cell modeling and parametrization based on the experimental characterization of real-life battery dynamics. The cell model contains the experimental data of the three first-life prismatic format cells (namely, NMC 1st life, LTO 1st life, and LFP 1st life) and one second-life LFP pouch format cell (namely, LFP 2nd life).

The electric behavior of cells is modeled with an electro-thermal model. This model couples an electric equivalent circuit model and a thermal model. The constant RC equivalent circuit model is derived from the classical electric equivalent circuit (EEC) model of lithium-ion battery cells [29–33]. This model is made of a DC voltage source, which models the variation of open circuit voltage (OCV) as a function of the state of charge (SoC), in series with a variable resistor R_0, which models the cell's internal resistance. To better model the dynamic voltage behavior of the cell, extra RC parallel blocks are added in series, as shown in Figure 7. A $\tau_i = R_i C_i$ value is defined for each RC block, depending on the dynamics of the current profiles applied to the model during the simulation of the HBESS. Each RC parallel block represents a different timescale response under current variation. Hence, the number of blocks is defined manually, as well as the $\tau_i = R_i C_i$ values. Then, during the model parameters identification process, only R_i values are fitted by the algorithm. It allows a faster identification process (C_i values are calculated from the equation $\tau_i = R_i C_i$).

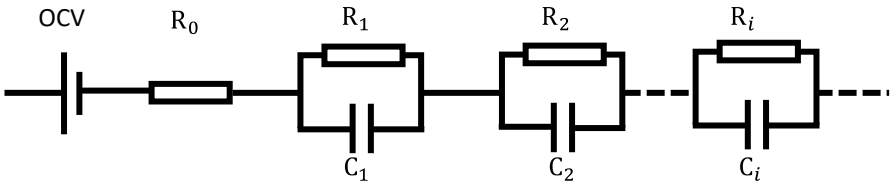

Figure 7. Equivalent circuits model of battery cells.

The model parameter dependencies are:

- OCV depends on SoC and temperature, but temperature dependency is considered negligible for a medium-fidelity model over SoC dependency [33].
- R_0, R_n, and C_n parameters depend on cell SoC, cell temperature, cell C-rate (charge and discharge current), and cell SoH (state of health).

A simple cell electro-thermal model is used to estimate the cell temperature variation. It is based on three equations:

- Joule losses: heat generation inside the cell:

$$Q_{in}(t) = \sum_{i=0}^{i=n} R_i I_{cell}^2(t) \quad (1)$$

- The thermal exchange between the cell and its surrounding environment:

$$Q_{out}(t) = h \cdot S \frac{dT(t)}{dt} \quad (2)$$

- Thermal energy transfer through the cell:

$$T = \int \frac{Q_{in}(t) - Q_{out}(t)}{mC_p} dt \quad (3)$$

where $Q(t)$ [W] is the thermal power; T [K] is the cell temperature, assumed homogeneous inside the cell; m [K] is the mass of the cell; C_p [J·K^{-1}·Kg^{-1}] is the specific heat capacity of the cell; S [m^2] is the exchange surface of the cell; h [W·m^{-2}·K^{-1}] is the heat transfer coefficient of the cell; and the m, C_p, and S parameters' values are measured experimentally. The h parameter value depends on the cooling and thermal architecture of the battery pack. Typical values are 1 to 10 for air (stationary or forced convection) and 10 to 1000 for water (stationary or forced convection).

The model parameters are identified by testing each selected cell with current pulses under several SoC, temperature, and current conditions and fitting the model behavior to the laboratory test data. The test results of OCV over SoC for the LIB cells are shown in Figure 8. The cell specifications that are used in this article are presented in Table 2.

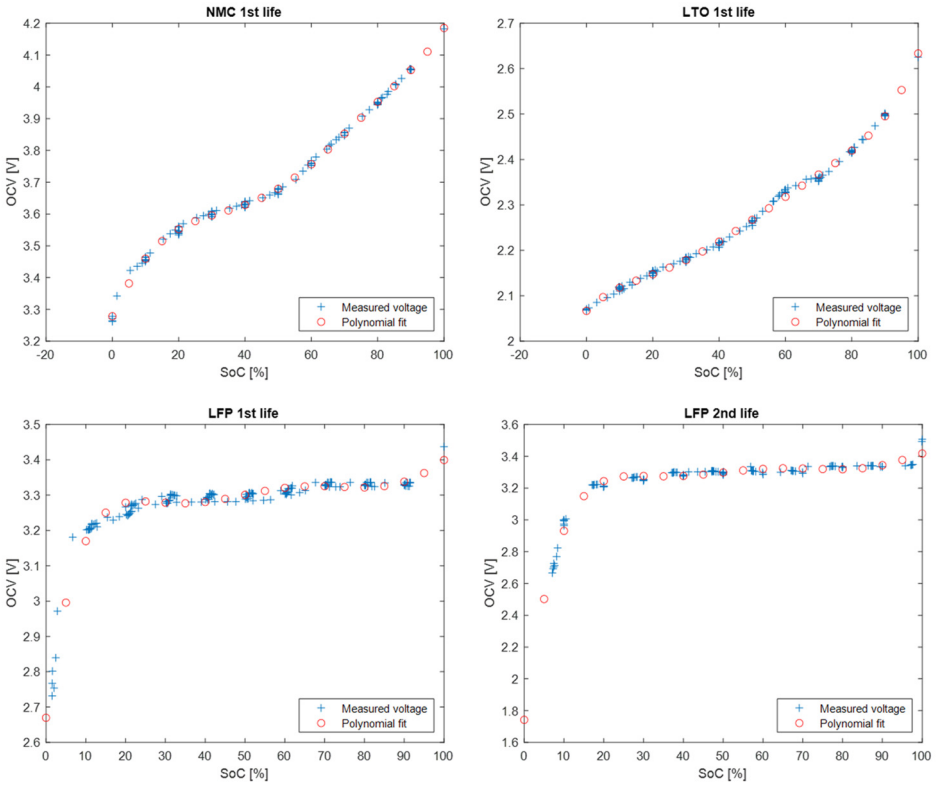

Figure 8. OCV identification result for the selected Li-ion cells in the COF.

Table 2. Selected cell specifications to be used in the COF.

Technology	NMC 1st Life	LTO 1st Life	LFP 1st Life	LFP 2nd Life
Nominal capacity [Ah]	51	20	280	20
Nominal voltage [V]	3.65	2.3	3.2	3.3
Max/min voltage [V]	4.2–2.5	2.7–1.5	3.65–2.5	3.8–1.6
Format	Prismatic	Prismatic	Prismatic	Pouch
Mass [g]	925	550	5220	496
Parametrized C-rate	−2C to +2C	−2C to +2C	−1C to +1C	−2C to +2C
Lifecycle at 80% DOD for 25 °C	1429	14,000	4530	4000
Cost [EUR/kWh]	200	500	260	180

The prepared parametrized battery model inputs are either power or current profiles and an ambient temperature profile, while outputs can be configured as module/pack

voltages, powers, currents, temperatures, energy losses, and the SoC of the battery pack by changing the number of cells in series (N_s) and number of cells in parallel (N_p). In this paper, using these model outputs, the respective efficiency (η) of different LIB cell technologies have been estimated using Equation (4), where P_{bat} and $P_{bat.loss}$ represent the output module power and losses, respectively. The absolute value is taken to cover both charging and discharging of the battery.

$$\eta_{bat} = \frac{\left| \int_{t=o}^{t} P_{bat} dt \right|}{\left| \int_{t=0}^{t} P_{bat} dt \right| + \left| \int_{t=0}^{t} P_{bat.loss} dt \right|} \tag{4}$$

Battery Lifetime Estimation Modeling

The lifetime of the system is more dependent on the battery packs than on the PE interfaces because a battery is more likely to hit its end of life, on average, than a power MOSFET is likely to fail. Thus, it is necessary to determine the lifetime of the BESS based on the full equivalent cycles (FEC) it is subjected to. The most common method of determining the *FEC* of the battery is through the cycle counting algorithm shown in Equation (5).

$$FEC = \frac{1}{2}\left(\frac{\sum_{t=1}^{T} E_{bat}(t) - E_{bat}(t-1)}{DoD(max) * S_{bat}} \right) \tag{5}$$

where E_{bat} is the cumulative charging and discharging energy over a period, T, and S_{bat} is the total energy content of the battery in kWh. The *FEC* is related to the SoH of the battery as a ratio of the battery's current cycle life to the maximum cycle life taken from the literature [34,35] being conservative in terms of tested C-rate. The maximum cycle life considered for the batteries is shown in Table 2. By convention, the end of the first life of a battery is reached when the capacity of a battery degrades by more than 80%, while the second life of the battery ends below 60% capacity degradation. The LFP 2nd-life battery considered here is assumed to have a 90% SoH and its cycle life is calculated based on the datasheet of its kind.

3.2. PCS Model

The COF uses the low-fidelity (LoFi) model of the PCS rather than the high-fidelity (HiFi) model to ensure faster system-level optimization simulation [36]. To consider the lifetime of the PCSs in the optimization, the LoFi models are extended with a fast electro-thermal model and analytical reliability assessment. The absolute worst-case reliability scenario has been modeled with regard to the PE system.

Generally, the HiFi models are employed for the physics-of-failure-based assessment and detailed characteristics test (e.g., dv/dt, short-circuit analysis) of the optimized PCS [36]. In contrast, the LoFi model is used for optimizations where simulation speed is critical. LoFi models combine a lookup table (LuT) and efficiency map from experimental test data alongside basic functional equations.

In this paper, the LoFi models for both power electronics interfaces (DC/DC and DC/AC converters) are based on efficiency (η) maps that are obtained from the original equipment manufacturer as a function of the battery voltage, DC-link voltage, and load power demand for their respective power converter test. Equations (6)–(9) describe the LoFi power flow model for the PCS-1 AC/DC module, while Equations (10)–(12) describe the power flow model for the PCS-2 AC/DC module, and Equations (13)–(15) describe the power flow model for the PCS-2 DC/DC module/power stage. The equations for power losses of PCS-1 and PCS-2 architecture are shown in Equations (9) and (16), respectively. The generic thermal model for the power electronics modules is shown in the next section.

$$\eta_{PCS-1} = LuT(V_{bat},\ P_{bat}) \tag{6}$$

$$P_{bat} = \begin{cases} P_{grid} * \eta_{PCS-1}, & P_{grid} < 0 \\ \frac{P_{grid}}{\eta_{PCS-1}}, & P_{grid} \geq 0 \end{cases} \quad (7)$$

$$I_{bat} = \frac{P_{bat}}{V_{bat}} \quad (8)$$

$$P_{loss\_PCS1} = \left| P_{bat} - P_{grid} \right| \quad (9)$$

$$\eta_{pcs-2(ac/dc)} = LuT(V_{dclink}, P_{dclink}) \quad (10)$$

$$P_{dclink} = \begin{cases} P_{grid} * \eta_{pcs-2(ac/dc)}, & P_{grid} < 0 \\ \frac{P_{grid}}{\eta_{pcs-2(ac/dc)}}, & P_{grid} \geq 0 \end{cases} \quad (11)$$

$$I_{dclink} = \frac{P_{dclink}}{V_{dclink}} \quad (12)$$

$$\eta_{pcs-2(dc/dc)} = LuT(V_{dclink}, I_{dclink}, V_{batt}) \quad (13)$$

$$P_{bat} = \begin{cases} P_{dclink} * \eta_{pcs-2(dc/dc)}, & P_{dclink} < 0 \\ \frac{P_{dclink}}{\eta_{pcs-2(dc/dc)}}, & P_{dclink} \geq 0 \end{cases} \quad (14)$$

$$I_{bat} = \frac{P_{bat}}{V_{bat}} \quad (15)$$

$$P_{loss\_PCS2} = |P_{bat} - P_{dclink}| + \left| P_{dclink} - P_{grid} \right| \quad (16)$$

where η_{PCS-1} is the efficiency of PCS-1 architecture; P_{bat} is the charging or discharging load power in the battery side; V_{bat} is the battery voltage; P_{grid} is the load request by the grid; I_{bat} is the battery current; P_{loss_PCS1} is the power loss of the PCS-1 architecture; $\eta_{pcs-2(ac/dc)}$ is efficiency of the AC/DC module in PCS-2 architecture; P_{dclink} is the internal power of the dc-link bus in the PCS-2 architecture; V_{dclink} is the dc-link voltage; I_{dclink} is the dc-link current; $\eta_{pcs-2(dc/dc)}$ is the efficiency of the DC/DC module of PCS-2; and P_{loss_PCS2} is the power loss of the PCS-2 architecture.

3.2.1. Electro-Thermal Modelling

Power semiconductors and their packaging are subject to several failure mechanisms, such as bond wire lifting and solder wear-out, and solder plate fatigue on the base plate and in the chip soldering. Among these, bond wire-related failures are the most prominent cause of power module failures [37]. These are caused by the repetitive thermo-mechanical stress induced by the temperature gradients between the components caused by the dissipated heat losses [38]. Therefore, the MOSFET junction temperature estimation is utilized to estimate the lifetime of the PCS. The thermal estimation equations are given in Equations (17)–(19) [39].

$$R_{tot} = \frac{\gamma}{Q} + \delta \quad (17)$$

$$\Delta T = P_{loss} * R_{tot} \quad (18)$$

$$T_{max} = \Delta T + T_{amb} \quad (19)$$

where R_{tot} is the total thermal resistance, and γ and Q are the coefficients to characterize the thermal resistance. The temperature difference (ΔT) is calculated by multiplying the generated power losses (P_{loss}) in terms of heat and R_{tot}; the maximum temperature (T_{max}) of the electrical component can be derived by the summation of ΔT and the ambient temperature of the system (T_{amb}).

3.2.2. System-Level Lifetime Estimation Modelling

This subsection seeks to estimate the system mean time between failures (MTBF) to evaluate the potential reliability of the modular PCS. This will assist in directing and planning for reliability and related program efforts and identifying design features critical to reliability. The reliability prediction method used in this analysis is taken from MIL-HDBK-217F(N1/2) [40]. The mathematical model used in determining the converter reliability is known as the series model. This model is based on Equations (20) and (21), where $R(t)$ is the overall reliability of the converter, t is the elapsed operation time (h), and λ is the constant failure rate.

$$R(t) = e^{-\lambda t} = e^{-\frac{t}{MTBF}} \tag{20}$$

$$\lambda = 1/MTBF \tag{21}$$

The reliability calculation of the PCS only considers the power semiconductors (i.e., a discrete SiC MOSFET, 1200 V, 115 A, 16 mΩ, Gen 3), which are the most failure-prone devices in PCSs [41]. The quality of the parts for the converter has been selected as MIL specified quality, but with a lower π_Q factor since they are sourced commercially. The reliability model includes the effects of environment stresses through the environmental factors, π_E, which for this paper has been selected to represent the ground, fixed type of environment. Moreover, the temperature response is taken from the thermal analysis for the worst ambient temperature (45 °C). The maximum range is fixed based on the thermal response of the PCS for the worst mission profile. If the PCS lifetime satisfies during the worst condition, it is evident that the lifetime will be higher for normal conditions. In Equation (22), the lifetime calculation for a MOSFET is presented.

$$\begin{gathered} \lambda_p = \lambda_b \cdot \pi_T \cdot \pi_Q \cdot \pi_E \cdot \pi_A \cdot \pi_B \\ \text{where } \pi_T = e^{-\frac{Ea}{k} * \left(\frac{1}{Tj+273} - \frac{1}{298}\right)};\ k = 8.6173303 * 10^{-5}. \end{gathered} \tag{22}$$

Please note that, the overall part failure rate, λ_p, of the individual components depends on a combination of the base failure rate, λ_b, and various stress modifiers including π_T (temperature factor), π_Q (quality factor), π_A (application factor), π_E (environment factor), and π_B (acceleration voltage breakdown).

The base failure rate is expressed by a model relating to the influence of electrical and thermal stresses on the MOSFET switch. The base failure rate is subjected to a modifier based on the power rating utilized by the MOSFET (π_A), on the category of environmental application such as whether the MOSFET is utilized in a marine or aerial or space, or ground (π_E), on the maximum junction temperature, Tj, expressed during the load profile, as given by T_{max} in Equation (19) (π_T), the level of quality at which the manufacturing process of the MOSFET is accomplished (π_Q), and the final influence on the stress modifier of the base failure rate is the breakdown voltage stress factor (π_B).These are considered from [40,41] for MOSFET lifetime formulation. The six switches (n = 6) in a series association are used in the convert power stages to estimate the PCS system-level lifetime. The system-level lifetime formula is given in Equation (23).

$$R(t) = \left(e^{-\lambda t}\right)^n \tag{23}$$

4. Framework Implementation

The COF is developed in a MATLAB/Simulink® modeling environment to describe the behavior of fully coupled HBESS. The framework is built in a modular approach shown in Figure 9 and consists of an input layer and a programming layer for the flexibility of the framework operation. The input layer asks for the input from the user for design specifications and constraints and database selection for intended system components and connection topology, followed by selection criterion. The programming layer interfaces the input data and the component model with a specific system model configuration for simula-

tion (with a selected connected topology) to the final output with an iterative optimization routine and decision-making criterion. The optimization routine incorporates a co-design method with multi-objective features and an evolutionary optimizer that identifies the Pareto front or feasible solution that satisfies all the constraints and requirements of the HBESS design. This section details the development of the optimization framework for HBESS. The core tasks of the COF are summarized as follows:

- Sizing battery packs with optimal cell configuration by respecting all the system subcomponents' specifications and constraints.
- Sizing the PCSs in terms of rating and number of modules in a connection topology.
- Finding the global optimal solution for HBESS from the selected connection topology defined in Section 2.1.

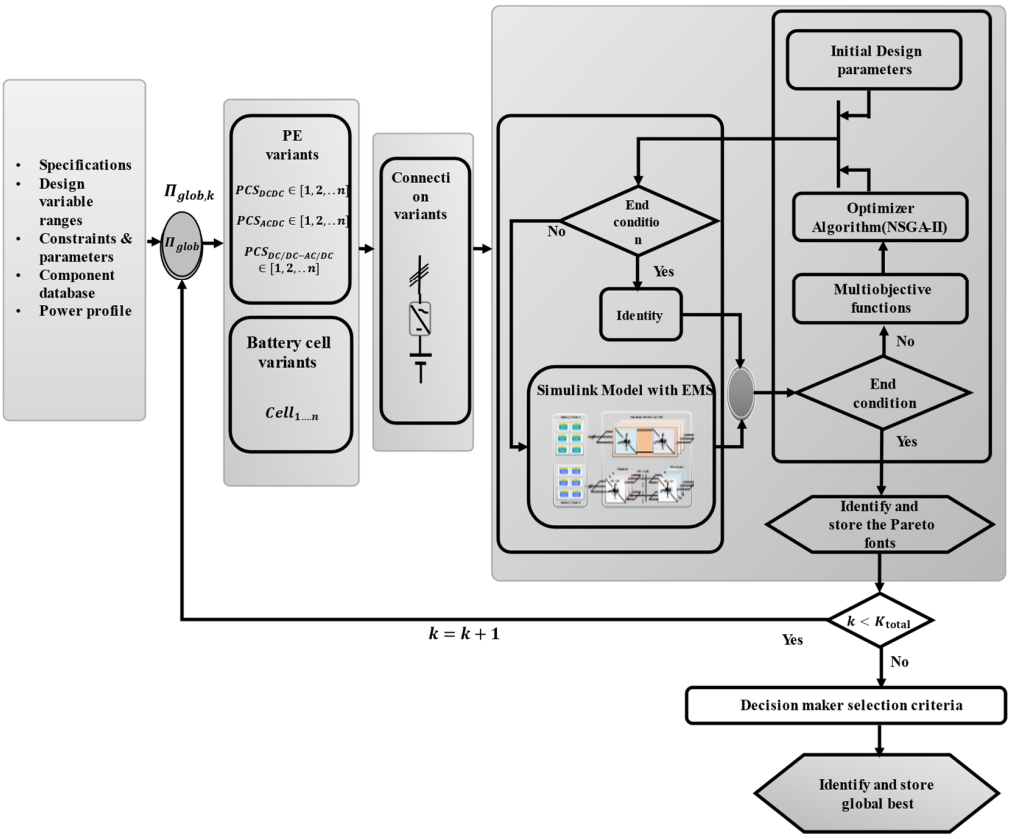

Figure 9. Methodology of COF for sizing and selection of technology toward optimal HBESS design.

4.1. Co-Design Optimization Problem Formulation

Oversizing a battery pack by adding extra cells in series or parallel to increase system life and roundtrip efficiency impacts the system investment cost as it bears a major part of the BESS cost. However, lowering the energy content can reduce the investment cost but increase the average C-rate while in operation. This increase in C-rate may have an effect on the roundtrip efficiency of the system, which in turn may have an effect on the operational cost. Additionally, since the service or use case power requests can be instantaneous or marathon in nature, the SoC of the battery can be influenced by overcharging or undercharging a battery pack, which can affect the battery life as well. Please note that battery pack sizing also requires us to respect the PCS voltage and current rating while in operation and PCS is expected to run for higher efficiency and lower stress. In a BESS, the EMS determines each battery pack's state (SoC and temperature) and also controls the power flow via the PE interfaces, in function of the allowed battery C-rate. So, to size the HBESS optimally, a simultaneous (SIM) co-design method has been used that guarantees a system level optimization [42]. The SIM co-design optimization problem

for HBESS can be formulated as Equation (24), with a sizing plant and control plant. The control plant ensures the power sharing between two battery packs in function of their C-rate and SoC to meet the use case power profile. The dynamics of power sharing are adopted from ref. [43].

$$\begin{gathered} \underset{x\epsilon(d_s,d_c)}{min} \quad F(x) = [f_1(x), f_2(x), f_3(x), f_4(x)] \\ \text{Subject to } g_i(x) \leq 0 \\ X = \{x | g_m(x) \leq 0, m = 1, 2, 3, \ldots . M\} \\ S = \{F(x | x \in X)\} \end{gathered} \tag{24}$$

where x represents the vector of design variables comprised of control plant variables (d_c) and system variables (d_s); $g_i(x)$ is the inequality constraints vector for control plant and system variables and m is the number of inequality constraints, X denotes the feasible decision space, and S is the criterion space. The objective functions are deemed to be either maximized or minimized; the ones to be maximized are reflected to be minimized. In addition, vector x contains the number of cells in series and parallel for each battery pack, the DC link voltage for PCS-2 architecture, two distinct PCS ratings, the capacity of the battery packs, their SoC, and their maximum C-rates. The problem is also formulated as a mixed-integer problem where the number of cells in the battery and the number of modules in the PCS are discrete numbers while other design variables are continuous.

4.2. Multi-Objective Function

In the framework, to assess the economic viability of the HBESS while sizing and selecting the technology, the IEC60300-3-3 [44] standard has been taken into consideration, which consists of six cost components: (1) concept and definition, (2) design and development, (3) manufacturing, (4) installation, (5) operation and maintenance, and (6) disposal. These components are aggregated into capital expenditure cost (CAPEX) as outcome of 1, 2, 3, 4, and operational and maintenance cost (OPEX) to evaluate the TCO. It should be noted that the disposal cost of the batteries is included in their CAPEX and not considered separately for this study.

The multi-objective functions used in the framework are prepared in a structure so that the combination of different batteries and PE configurations can be evaluated in the same fashion.

The system economic objective is considered with the TCO, which is the summation of the CAPEX and OPEX. The CAPEX is calculated using Equation (25). Only power electronics and battery costs have been considered in the CAPEX as they directly affect the system design optimization outcome. The TCO is set with 10 years of service life as in ref. [45] to consider the influence of the system operation for a standard stationary energy storage system lifetime.

$$CAPEX = (C_{PE1} \times P_{m \cdot PE1} \times N_{PE1} + C_{PE2} \times P_{m \cdot PE2} \times N_{PE2}) + (C_{BAT1} \times E_{BAT1} + C_{BAT2} \times E_{BAT2}) \tag{25}$$

where C_{PE1} and C_{PE2} are the costs of PE interfaces for PCS-1 and PCS-2, respectively [EUR/kW]; $P_{m \cdot PE1}$, $P_{m \cdot PE2}$ are the modules rated power of the PE interfaces [kW]; N_{PE1}, N_{PE2} are the numbers of modules of the PE interfaces; C_{BAT1}, C_{BAT2} are battery pack-1 and pack-2 costs, respectively [EUR/kWh], and E_{BAT1}, E_{BAT2} are the capacities of the battery pack-1 and pack-2, respectively [kWh].

The OPEX is calculated using Equation (26). In the OPEX, the potential battery replacement cost during the 10 years of operation has been considered with an 8% annual reduction of battery price up to 2030. However, in this study, the residual value of the

systems (mainly the first-life batteries) is not considered, but it could be utilized while estimating the levelized cost of the storage systems.

$$OPEX = \sum_{y=1}^{y=10yrs} \left(E_{tariff} \times E_{tot} \times \eta'_{sys} + r_c \right) \tag{26}$$

$$f_1 = TCO = CAPEX + OPEX \tag{27}$$

where E_{tariff} is the energy tariff of EU-27 in 2019 and amounts to 0,13 EUR/kWh [46]; E_{tot} is the total energy request in [kWh]; η'_{sys} is the complement of the η_{sys}; and r_c is the replacement cost in [EUR].

The efficiency of the HBESS is estimated based on the efficiency of the two independent battery packs and their connected PCSs. The average system roundtrip efficiency is calculated as in Equation (28).

$$f_2 = \eta_{sys} = \frac{(\eta_{PE \cdot B1} \cdot \eta_{B1} + \eta_{PE \cdot B2} \cdot \eta_{B2})}{2} \tag{28}$$

where $\eta_{PE \cdot B1}$, $\eta_{PE \cdot B2}$ are the efficiencies of the PE interfaces connected to battery pack-1 and pack-2, respectively; η_{B1}, η_{B2} are the efficiencies of battery pack-1 and pack-2, respectively.

The lifetime of each battery and PCS has been estimated using Equations (29) and (30), as discussed in Section 3. In this task, 365 days have been considered for operation within one year. The objective is to maximize the lifetime of both the battery packs (f_3) and the PCS interfaces (f_4).

$$f_3 = Bat_{lifetime} = cyclelife/(cycle \times operating\ days) \tag{29}$$

$$f_4 = R(t) = \left(e^{-\lambda t} \right)^6 \tag{30}$$

4.3. Variables and Constraints

The constraints define conditions for variables for the designing system components that must be met. Tables 3 and 4 present/summarize the explicit constraint/variables for PCS-1 and PCS-2 architecture for the HBESS, where the battery packs will be sized to satisfy an application with nominal power of 100 kW and nominal capacity of 100 kWh with an upper margin of 15%. Any power electronics interface must respect the constraints of the energy storage system as mentioned in Table 2, especially its C-rate and its SoC, which is capped at 80% since the batteries are always assumed to operate in the constant current mode.

Table 3. Specifications and constraints for PCS- 1.

Constraints/Variables	Description
$idx_{bat} \in [1, 2 \ldots n]$	N variants of battery types
$idx_{ACDC} \in [1, 2, 3 \ldots n]$	N variants of DC/AC module combinations
$100 \leq Batt_{voltage} \leq 200$	Battery voltage range
PE stage efficiency $\geq 98\% * 98\%$	Power electronics efficiency input to output, half to full power

Specifications for PCS-1: Max. current rating per module is 200 A; Power rating per module is 25 kW.

Table 4. Specifications and constraints for PCS-2.

Constraints/Variables	Description
$idx_{bat} \in [1, 2 \ldots n]$	N variants of battery types
$idx_{DCDC} \in [1, 2, 3 \ldots n]$	N variants of DC/DC converter combinations
$idx_{ACDC} \in [1, 2, 3 \ldots n]$	N variants of DC/AC converter modularity
700 V $\leq V_{DClink} \leq$ 800 V	DC-Link voltage range
$300 \leq Batt_{voltage} \leq 400$	Battery voltage range
PE stage efficiency $\geq 98\% * 98\%$	Power electronics efficiency input to output, half to full power

Specifications for PCS-2: power rating per module (DC/AC) is 33 kVA; power rating per module (DC/DC) is 15 kW–20 kW; max. current per module (DC/DC) is 50 A.

4.4. Optimizer Selection

The optimization of the HBESS is a complex and nonconvex problem. Therefore, to keep the flexibility in decision-making without giving complete control to the algorithm to decide the final result, NSGA-II is considered in the task as NSGA-II uses a Pareto-front hierarchy and adopts an elitism mechanism to retain the best solutions generated during the search [47]. According to the study [48] carried out in a similar kind of problem-solving, NSGA-II gives more accurate results but is slightly slower than other multi-objective optimizers such as PSO. Since the COF is not developed for a real-time operation, it does not require a fast response, and priority is given to accuracy. Besides, by nature, GA performs an efficient and parallelizable search. Moreover, a similar characteristics system optimization problem has also been performed with the adopted algorithm [49,50] for its capacity to evolve solutions with multi-objective functions with discrete and continuous design variables. The NSGA-II algorithm, integer crossover, and mutation operator for a mixed-integer problem are well described and adapted from [51]. For iterative optimization run the optimizer is set with the following settings in this work for each possible combination in the connection topology:

- Population size: 100
- Crossover: simulated binary
- Mutation: Gaussian distribution
- Number of generations: 25
- Stall generation limit: 50

4.5. Selection Criterion

When a number of Pareto optimal solutions are found after one successful complete iterative optimization routine, then to find the best solution among all feasible solutions, a composite function in Equation (31) is applied with different weighting factors for each objective based on their importance in the final HBESS solution. The weighted sum of the various objective functions is given by:

$$O_{ws}(x) = \sum_{i=1}^{k} w_i f_i(x) \tag{31}$$

where $w_i \in [0, 1]$ are the weight factors assigned to each objective and $f_i(x)$ is normalized to [0,1], resulting in a dimensionless number. In this paper, the solution selection criterion is set as in Equation (32) for the global optimal HBESS design with sizing and selection:

$$S = 0.6 \cdot f_1(x) + 0.1 \cdot f_2(x) + 0.2 \cdot f_3(x) + 0.1 \cdot f_4(x) \tag{32}$$

where the system cost has a 60% weight; system efficiency has a 10% weight since the efficiency of system components is addressed before in the limitations; and battery lifetime has a higher percentage than PCS as battery replacement costs are higher.

5. Optimization Results

In this part, the results of the co-design optimization are presented for HBESS. The COF can be applied to each combination of battery packs and PE interfaces, totaling 16 combinations as indicated in Table 5.

Table 5. Combination among the cells and PCS configurations for global optimum selection and sizing of HBESS technology.

TO-1		**TO-2**		**TO-3**		**TO-4**	
LTO LFP	PCS-1 PCS-1	LTO LFP	PCS-2 PCS-2	LTO LFP	PCS-2 PCS-1	LTO LFP	PCS-1 PCS-2
C1		C5		C9		C13	
NMC LFP	PCS-1 PCS-1	NMC LFP	PCS-2 PCS-2	NMC LFP	PCS-2 PCS-1	NMC LFP	PCS-1 PCS-2
C2		C6		C10		C14	
LTO 2ndlife	PCS-1 PCS-1	LTO 2nd life	PCS-2 PCS-2	LTO 2nd life	PCS-2 PCS-1	LTO 2nd life	PCS-1 PCS-2
C3		C7		C11		C15	
NMC 2nd life	PCS-1 PCS-1	NMC 2nd life	PCS-2 PCS-2	NMC 2nd life	PCS-2 PCS-1	NMC 2nd life	PCS-1 PCS-2
C4		C8		C12		C16	

The framework is capable of selecting any defined connection topology selection (Section 2.1) toward the global optimal HBESS sizing and selection. In the framework, the selection of batteries for HBESS combinations is based on the categorization of cell characteristics, particularly C-rate. LTO and NMC cells are regarded for HP applications because of their high C-rate and low energy capacity, while LFP (1st- and 2nd-life) cells are chosen for energy-centric applications because of their large energy capacity and relatively low C-rate restrictions. Despite the fact that the LFP 2nd-life battery has a limited energy capacity, it has been classified as an energy-focused application to increase its remaining usable lifetime by restricting the C-rate.

For each combination within the selected connection topology, the NSGA(II) algorithm finds the Pareto fonts that size the design components toward lower cost and higher efficiency and lifetime. Then, the programming layer stores these fronts in the database for further post-processing and reiterates another combination within the same selected connection topology. The Pareto fronts produced from the framework for connection topology-1 (Figure 2) are illustrated in Figure 10. Then applying the defined selection criteria, for example, here in Equation (32), the best HBESS solutions and their sizes are generated in terms of the defined objective functions and stored in the COF result database as per the combinational name such as C1, C2, C3, and C4 for the connection topology, TO-1. The best combinational HBESS solutions obtained from the framework result database for the TO-1 are presented in Table 6. Please note that a similar approach is followed if different topologies are selected in the framework at once.

To find the global optimal solution the same selection criteria is applied to the saved best optimal solution set by normalizing the multi-objective functions of the solution set. The normalized values for C1, C2, C3, and C4 are illustrated in Figure 11. The framework then finds the lowest value in the normalized solution set. The lowest value in the connection topology-1 indicates that solution C3, consisting in the use of LTO and second-life battery technologies, is the global optimum solution among the four possible hybridizations considered in the framework. It should be noted that different selection criteria with different weights can lead to different best/global optimum solutions; also, since in the used selection criteria the system cost carries the highest share of the weights, the system components' cost will have an influence toward the best optimal solution.

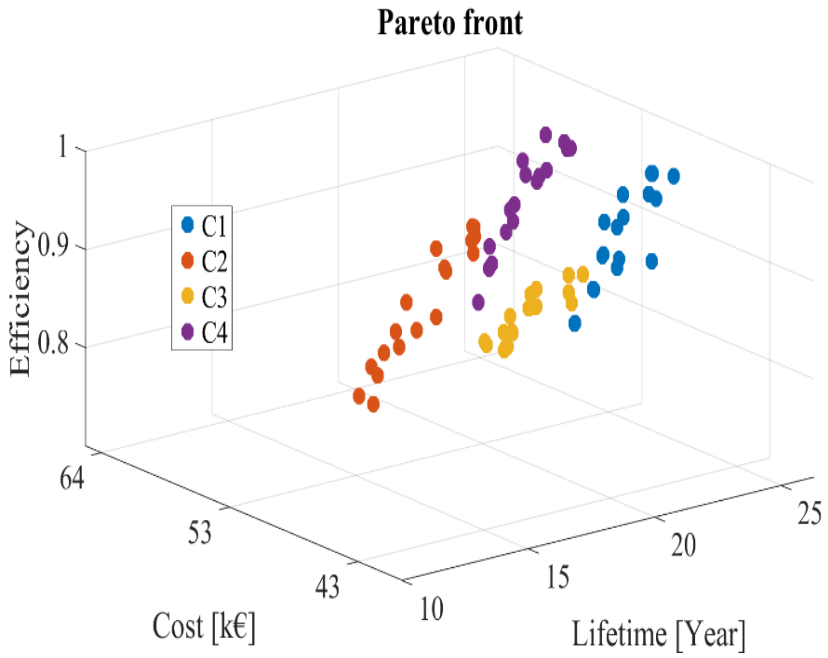

Figure 10. Pareto-optimal HBESS solutions found by the COF for TO-1.

Table 6. Optimal hybrid system configuration solutions with the topology, TO-1.

HBESS Sol^n	Cell Tech.	$N_s \times N_p$	V_{Nom} (V)	E_{bp}(kWh)	P_m^{pe1}(kVA)	N_m^{pe1}
C1	LTO	72s15p	162	48.6	25	2
	LFP	60s1p	192	53.76		2
C2	NMC	42s6p	153	45.9	25	2
	LFP	60s1p	192	53.76		2
C3	LTO	69s8p	158.7	25.392	25	1
	2nd life	56s22p	174.9	76.95		3
C4	NMC	42s6p	153	45.9	25	3
	2nd life	56s18p	184	55.2		1

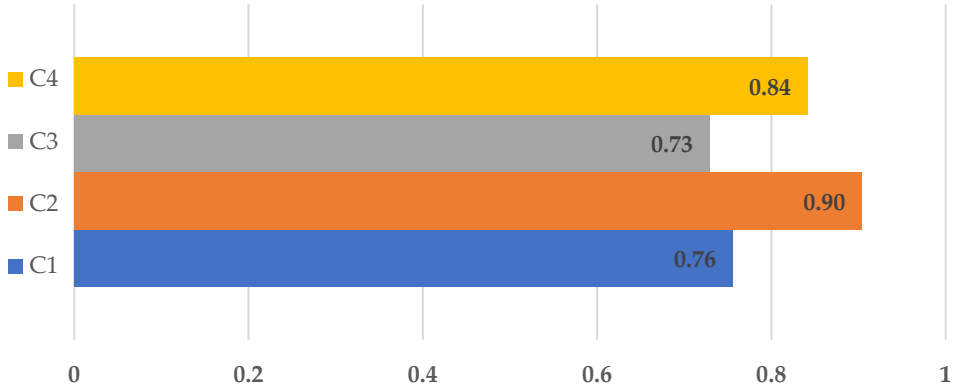

Figure 11. Normalized values of selection criterion applied to saved best optimal Pareto fronts.

However, a baseline comparison is carried out to assess the optimality of the obtained solution from the framework in terms of TCO and system efficiency for TO-1. For the baseline, each battery pack is sized with a nominal power of 50 kW as an equally balanced system to reach the previously mentioned system target of 100 kW/100 kWh. In the

baseline, the sizing of the battery pack is first made based on the voltage operation defined by the PCS-1 (Table 3) and then on the maximum power and energy required for the designed system. The results of the sizing of each battery pack for the baseline comparison are presented in Table 7.

Table 7. Baseline HBESS configurations.

Baseline HBESS Sol^n	Cell Tech.	$N_s \times N_p$	V_{Nom} (V)	E_{bp}(kWh)
B1	LTO	72s17p	165.6	56.304
	LFP	53s1p	169.6	47.488
B2	NMC	42s6p	169.2	51.77
	LFP	60s1p	172.8	48.384
B3	LTO	72s15p	165.6	56.3
	2nd life	56s15p	178.2	49.896
B4	NMC	42s6p	169.2	51.77
	2nd life	56s18p	181.5	50.82

The baseline comparison in terms of TCO and system roundtrip efficiency with the obtained optimized solution is illustrated in Figure 12. Please note that during the assessment of TCO and system efficiency, the sizing from baseline and COF is evaluated under similar conditions by using the framework simulation models and power-sharing principle and by respecting all the PCS-1 constraints. The optimal sizing from the COF for C1, C2, C3, and C4 reduces the TCO by 29.3%, 12.3%, 29.6%, and 16.2%, respectively, compared to the baseline solutions; also, the system round trip efficiency is improved by 4.2%, 4.4%, 4.7%, and 5% against the baseline sizing for B1, B2, B3, and B4, respectively, which confirms the relevance of the co-design optimization framework.

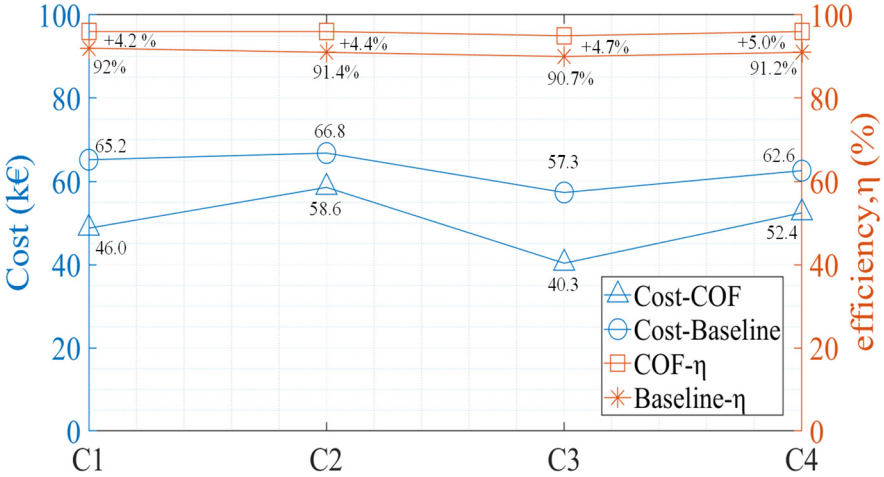

Figure 12. Comparison of the obtained optimal sizing from COF and baseline for HBESS solutions.

6. Conclusions

This paper presents the development of a holistic and flexible framework for sizing and selecting the significant components of an HBESS by simulating such coupled and nonlinear systems iteratively. The framework supports several LIB cell technologies. In this study, four different types of cells are used to construct hybrid battery packs and their solutions are evaluated on a techno-economic scale. In addition, the framework provides four distinct HBESS-to-grid topologies and two unique PE architectures, which enable the flexibility of incorporating the commercial single-stage bidirectional PCS or bidirectional two-stage converter with a common DC link, or both, while sizing the coupled

HBESS within the discussed variables and constraints for bi-directional grid service power profile. Besides, the NSGA-II algorithm and multi-objective selection criteria adopted in the framework help to reach the globally best solution based on any selected connection topology and achieve lower system cost, improved system efficiency, and longer lifetime. The obtained result from the framework for the frequency service power profile shows that it can reduce the TCO by 29.3% for an HBESS made up of LTO and LFP cell chemistries; 12.3% for the solution comprised of NMC and LFP cells; 29.6% for LTO and LFP 2nd-life cells; and 16.2% for NMC and LFP 2nd-life cells.

All in all, such a framework has high relevance in the design and techno-economic analysis of HBESSs, as these come with a large number of (iterative) simulations. Thus, the presented co-design optimization framework for automated simulation and optimization forms the basis for optimally sizing and selecting the HBESS subcomponents for grid applications.

Author Contributions: Methodology, M.M.H., S.C., T.G. and O.H.; software, M.M.H.; resources, B.B., T.M. and I.C.; writing—original draft preparation, M.M.H.; writing—review and editing, B.B., T.M., I.C., S.C., T.G. and O.H.; supervision, T.G. and O.H. All authors have read and agreed to the published version of the manuscript.

Funding: This project has received funding from the European Union's Horizon 2020 research and innovation program under grant agreement No. 963527 (iSTORMY).

Data Availability Statement: Not applicable.

Acknowledgments: The authors would like to acknowledge the iSTORMY consortiums for providing their valuable inputs. Authors also acknowledge the Flanders Make for their support to the MOBI-EPOWERS research group.

Conflicts of Interest: The authors declare no conflict of interest.

References

1. Challenge, Energy Storage Grand. In *Energy Storage Market Report*; US Department of Energy: Washington, DC, USA, 2020.
2. Lebedeva, N.; Tarvydas, D.; Tsiropoulos, I.; European Commission; Joint Research Centre. *Li-Ion Batteries for Mobility and Stationary Storage Applications: Scenarios for Costs and Market Growth*; Publications Office of the European Union: Luxembourg, 2018.
3. Mongird, K.; Viswanathan, V.V.; Balducci, P.J.; Alam, M.J.E.; Fotedar, V.; Koritarov, V.S.; Hadjerioua, B. *Energy Storage Technology and Cost Characterization Report (No. PNNL-28866)*; Pacific Northwest National Lab. (PNNL): Richland, WA, USA, 2019.
4. European Commission. *SET-Plan ACTION n 7–Declaration of Intent "Become Competitive in the Global Battery Sector to Drive e-Mobility Forward"*; European Commission: Brussels, Belgium, 2016; pp. 1–9.
5. Diaz, P.M.; El-Khozondar, H.J. Electrical energy storage technologies and the application potential in power system operation: A mini review. In Proceedings of the IEEE 7th Palestinian International Conference on Electrical and Computer Engineering (PICECE), Gaza, Palestine, 26–27 March 2019.
6. Ferreira, H.L.; Garde, R.; Fulli, G.; Kling, W.; Lopes, J.P. Characterisation of electrical energy storage technologies. *Energy* **2013**, *53*, 288–298. [CrossRef]
7. Yao, L.; Yang, B.; Cui, H.; Zhuang, J.; Ye, J.; Xue, J. Challenges and progresses of energy storage technology and its application in power systems. *J. Mod. Power Syst. Clean Energy* **2016**, *4*, 519–528. [CrossRef]
8. Arias, N.B.; López, J.C.; Hashemi, S.; Franco, J.F.; Rider, M.J. Multi-objective sizing of battery energy storage systems for stackable grid applications. *IEEE Trans. Smart Grid* **2020**, *12*, 2708–2721. [CrossRef]
9. Chen, T.; Jin, Y.; Lv, H.; Yang, A.; Liu, M.; Chen, B.; Xie, Y.; Chen, Q. Applications of lithium-ion batteries in grid-scale energy storage systems. *Trans. Tianjin Univ.* **2020**, *26*, 208–217. [CrossRef]
10. Choi, W.; Wu, Y.; Han, D.; Gorman, J.; Palavicino, P.C.; Lee, W.; Sarlioglu, B. Reviews on grid-connected inverter, utility-scaled battery energy storage system, and vehicle-to-grid application-challenges and opportunities. In Proceedings of the 2017 IEEE Transportation Electrification Conference and Expo (ITEC), Chicago, IL, USA, 22–24 June 2017.
11. Zhang, L.; Hu, X.; Wang, Z.; Ruan, J.; Ma, C.; Song, Z.; Dorrell, D.G.; Pecht, M.G. Hybrid electrochemical energy storage systems: An overview for smart grid and electrified vehicle applications. *Renew. Sustain. Energy Rev.* **2021**, *139*, 110581. [CrossRef]

12. McIlwaine, N.; Foley, A.M.; Morrow, D.J.; Al Kez, D.; Zhang, C.; Lu, X.; Best, R.J. A state-of-the-art techno-economic review of distributed and embedded energy storage for energy systems. *Energy* **2021**, *229*, 120461. [CrossRef]
13. Faessler, B. Stationary, Second Use Battery Energy Storage Systems and Their Applications: A Research Review. *Energies* **2021**, *14*, 2335. [CrossRef]
14. Kumar, R.; Channi, H.K. A PV-Biomass off-grid hybrid renewable energy system (HRES) for rural electrification: Design, optimization and techno-economic-environmental analysis. *J. Clean. Prod.* **2022**, *349*, 131347. [CrossRef]
15. Eldeeb, H.H.; Hariri, A.O.; Lashway, C.R.; Mohammed, O.A. Optimal sizing of inverters and energy storage for power oscillation limiting in grid connected large scale Electric Vehicle park with renewable energy. In Proceedings of the 2017 IEEE Transportation Electrification Conference and Expo (ITEC), Chicago, IL, USA, 22–24 June 2017; pp. 288–293. [CrossRef]
16. Klansupar, C.; Chaitusaney, S. Optimal Sizing of Utility-scaled Battery with Consideration of Battery Installtion Cost and System Power Generation Cost. In Proceedings of the 2020 17th International Conference on Electrical Engineering/Electronics, Computer, Telecommunications and Information Technology (ECTI-CON), Phuket, Thailand, 24–27 June 2020.
17. Takano, H.; Hayashi, R.; Asano, H.; Goda, T. Optimal Sizing of Battery Energy Storage Systems Considering Cooperative Operation with Microgrid Components. *Energies* **2021**, *14*, 7442. [CrossRef]
18. Zhou, N.; Liu, N.; Zhang, J.; Lei, J. Multi-Objective Optimal Sizing for Battery Storage of PV-Based Microgrid with Demand Response. *Energies* **2016**, *9*, 591. [CrossRef]
19. Bartolucci, L.; Cordiner, S.; Mulone, V.; Santarelli, M.; Lombardi, P.; Arendarski, B. Towards Net Zero Energy Factory: A multi-objective approach to optimally size and operate industrial flexibility solutions. *Int. J. Electr. Power Energy Syst.* **2022**, *137*, 107796. [CrossRef]
20. Hannan, M.A.; Wali, S.B.; Ker, P.J.; Abd Rahman, M.S.; Mansor, M.; Ramachandaramurthy, V.K.; Muttaqi, K.M.; Mahlia, T.M.I.; Dong, Z.Y. Battery energy-storage system: A review of technologies, optimization objectives, constraints, approaches, and outstanding issues. *J. Energy Storage* **2021**, *42*, 103023. [CrossRef]
21. Verma, S.; Millie, P.; Vaclav, S. A comprehensive review on NSGA-II for multi-objective combinatorial optimization problems. *IEEE Access* **2021**, *9*, 57757–57791. [CrossRef]
22. Fonseca, C.M.; Fleming, P.J. Multi-objective genetic algorithms. In Proceedings of the IEE Colloquium on Genetic Algorithms for Control Systems Engineering, London, UK, 28–28 May 1993; pp. 6/1–6/5.
23. Li, X.; Wang, S. Energy management and operational control methods for grid battery energy storage systems. *CSEE J. Power Energy Syst.* **2019**, *7*, 1026–1040.
24. Zhao, B.; Zhang, X.; Chen, J.; Wang, C.; Guo, L. Operation Optimization of Standalone Microgrids Considering Lifetime Characteristics of Battery Energy Storage System. *IEEE Trans. Sustain. Energy* **2013**, *4*, 934–943. [CrossRef]
25. Cupelli, L.; Barve, N.; Monti, A. Optimal sizing of data center battery energy storage system for provision of frequency containment reserve. In Proceedings of the IECON 2017-43rd Annual Conference of the IEEE Industrial Electronics Society, Beijing, China, 29 October–1 November 2017; pp. 7185–7190. [CrossRef]
26. Bereczki, B.; Hartmann, B.; Kertesz, S. Industrial Application of Battery Energy Storage Systems: Peak shaving. In Proceedings of the 7th International Youth Conference on Energy (IYCE), Bled, Slovenia, 3–6 July 2019; pp. 1–5. [CrossRef]
27. Hesse, H.C.; Schimpe, M.; Kucevic, D.; Jossen, A. Lithium-Ion Battery Storage for the Grid—A Review of Stationary Battery Storage System Design Tailored for Applications in Modern Power Grids. *Energies* **2017**, *10*, 2107. [CrossRef]
28. Hybrid Storage Systems and Use-Cases. Available online: https://istormy.eu/1-hybrid-storage-systems-and-use-cases-specifications-and-requirements/ (accessed on 1 March 2022).
29. Plett, G.L. *Battery Management Systems: Battery Modeling*; Artech House: London, UK, 2015; Volume 1.
30. Liu, G.; Lu, L.; Fu, H.; Hua, J.; Li, J.; Ouyang, M.; Wang, Y.; Xue, S.; Chen, P. A comparative study of equivalent circuit models and enhanced equivalent circuit models of lithium-ion batteries with different model structures. In Proceedings of the 2014 IEEE Conference and Expo Transportation Electrification Asia-Pacific (ITEC Asia-Pacific), Beijing, China, 31 August–3 September 2014; pp. 1–6. [CrossRef]
31. Barreras, J.V.; Pinto, C.; de Castro, R.; Schaltz, E.; Swierczynski, M.; Andreasen, S.J.; Araujo, R.E. An improved parametrization method for Li-ion linear static Equivalent Circuit battery Models based on direct current resistance measurement. In Proceedings of the 2015 International Conference on Sustainable Mobility Applications, Renewables and Technology (SMART), Kuwait City, Kuwait, 23–25 November 2015; pp. 1–9. [CrossRef]
32. Kowal, J.; Gerschler, J.B.; Schaper, C.; Schoenen, T.; Sauer, D.U. Efficient battery models for the design of EV drive trains. In Proceedings of the 14th International Power Electronics and Motion Control Conference EPE-PEMC 2010, Ohrid, Macedonia, 6–8 September 2010; p. 5606677. [CrossRef]
33. Farmann, A.; Sauer, D.U. A study on the dependency of the open-circuit voltage on temperature and actual aging state of lithium-ion batteries. *J. Power Sources* **2017**, *347*, 1–13. [CrossRef]
34. Irena.Org. 2021. Available online: https://www.irena.org/-/media/Files/IRENA/Agency/Publication/2017/Oct/IRENA_Electricity_Storage_Costs_2017.pdf (accessed on 19 November 2021).
35. Mongird, K.; Viswanathan, V.; Alam, J.; Vartanian, C.; Sprenkle, V.; Baxter, R. *2020 Grid Energy Storage Technology Cost and Performance Assessment*; US Department of Energy: Washington, DC, USA, 2020.

36. Chakraborty, S.; Mazuela, M.; Tran, D.-D.; Corea-Araujo, J.A.; Lan, Y.; Loiti, A.A.; Garmier, P.; Aizpuru, I.; Hegazy, O. Scalable Modeling Approach and Robust Hardware-in-the-Loop Testing of an Optimized Interleaved Bidirectional HV DC/DC Converter for Electric Vehicle Drivetrains. *IEEE Access* **2020**, *8*, 115515–115536. [CrossRef]
37. Yang, Y.; Wang, H.; Sangwongwanich, A.; Blaabjerg, F. 45-Design for Reliability of Power Electronic Systems. In *Power Electronics Handbook*; Butterworth-Heinemann: Oxford, UK, 2018; pp. 1423–1440.
38. Ruthardt, J.; Schulte, H.; Ziegler, P.; Fischer, M.; Nitzsche, M.; Roth-Stielow, J. Junction Temperature Control Strategy for Lifetime Extension of Power Semiconductor Devices. In Proceedings of the 22nd European Conference on Power Electronics and Applications (EPE'20 ECCE Europe), Lyon, France, 7–11 September 2020.
39. Park, H. Numerical assessment of liquid cooling system for power electronics in fuel cell electric vehicles. *Int. J. Heat Mass Transf.* **2014**, *73*, 511–520. [CrossRef]
40. *Military Handbook MIL HDBK 217F: Reliability Prediction of Electronic Equipment*; USA Department of Defense: Washington, DC, USA, 1991. Available online: http://snebulos.mit.edu/projects/reference/MIL-STD/MIL-HDBK-217F-Notice2.pdf (accessed on 10 April 2021).
41. Chakraborty, S.; Hasan, M.M.; Tran, D.D.; Jaman, S.; Bossche, P.V.D.; El Baghdadi, M.; Hegazy, O. Reliability Assessment of a WBG-based Interleaved Bidirectional HV DC/DC Converter for Electric Vehicle Drivetrains. In Proceedings of the Fifteenth International Conference on Ecological Vehicles and Renewable Energies (EVER), Monte-Carlo, Monaco, 10–12 September 2020.
42. Kamadan, A.; Kiziltas, G.; Patoglu, V. Co-Design Strategies for Optimal Variable Stiffness Actuation. *IEEE/ASME Trans. Mechatronics* **2017**, *22*, 2768–2779. [CrossRef]
43. Omar, N.; Fleurbaey, K.; Kurtulus, C.; Bossche, P.V.D.; Coosemans, T.; Van Mierlo, J. SuperLIB Project–Analysis of the Performances of the Hybrid Lithium HE-HP Architecture for Plug-In Hybrid Electric Vehicles. *World Electr. Veh. J.* **2013**, *6*, 259–268. [CrossRef]
44. Jeromin, I.; Balzer, G.; Backes, J.; Huber, R. Life cycle cost analysis of transmission and distribution systems. In Proceedings of the 2009 IEEE Bucharest PowerTech, Bucharest, Romania, 28 June–2 July 2009.
45. Marchi, B.; Zanoni, S.; Pasetti, M. A techno-economic analysis of Li-ion battery energy storage systems in support of PV distributed generation. In Proceedings of the 21st Summer School F. Turco of Industrial Systems Engineering, Naples, Italy, 13–15 September 2016.
46. Cambridge Econometrics:Cambridge Econometrics, Study on Energy Prices, Costs and Their Impact on Industry and HOUSEHOLDS: Final report. Op.Europa.eu. 2021. Available online: https://op.europa.eu/en/publication-detail/-/publication/16e7f212-0dc5-11eb-bc07-01aa75ed71a1 (accessed on 15 November 2021).
47. Deb, K.; Pratap, A.; Agarwal, S.; Meyarivan, T. A fast and elitist multi-objective genetic algorithm: NSGA-II. *IEEE Trans. Evol. Comput.* **2002**, *6*, 182–197. [CrossRef]
48. Hlal, M.I.; Ramachandaramurthya, V.K.; Padmanaban, S.; Kaboli, H.R.; Pouryekta, A.; Abdullah, T.A.R.B.T. NSGA-II and MOPSO based optimization for sizing of hybrid PV/wind/battery energy storage system. *Int. J. Power Electron. Drive Syst. (IJPEDS)* **2019**, *10*, 463–478. [CrossRef]
49. Tran, D.D.; Hegazy, O.; Van Mierlo, J.; Smijtink, R.; Hellgren, J.; Lindgarde, O.; Pham, T.; Wilkins, S. Modeling and Co-design Optimization for Heavy Duty Trucks. In Proceedings of the 31st International Electric Vehicles Symposium & Exhibition & International Electric Vehicle Technology Conference 2018, Kobe, Japan, 30 September–2 October 2018.
50. Chakraborty, S.; Padmaji, V.; Tran, D.-D.; Araujo, J.A.C.; Geury, T.; El Baghdadi, M.; Hegaz, O. Multi-objective GA Optimization for Energy Efficient Electric Vehicle Drivetrains. In Proceedings of the 2021 Sixteenth International Conference on Ecological Vehicles and Renewable Energies (EVER), Monaco City, Monaco, 5–7 May 2021.
51. Rainer, M. A genetic algorithm for mixed-integer multicriteria optimization problems and its application to engines in order to optimize fuel consumption and driving performance. Master Thesis, Graz University of Technology, Graz, Austria, 2012.